MAGNETISM

Topological kinetic crossover in a nanomagnet array

Xiaoyu Zhang[1], Grant Fitez[1], Shayaan Subzwari[1], Nicholas S. Bingham[1]†, Ioan-Augustin Chioar[1], Hilal Saglam[1], Justin Ramberger[3], Chris Leighton[3], Cristiano Nisoli[2]*, Peter Schiffer[1,4]*

Ergodic kinetics, which are critical to equilibrium thermodynamics, can be constrained by a system's topology. We studied a model nanomagnetic array in which such constraints visibly affect the behavior of the magnetic moments. In this system, magnetic excitations connect into thermally active one-dimensional strings whose motion can be imaged in real time. At high temperatures, our data showed the merging, breaking, and reconnecting of strings, resulting in the system transitioning between topologically distinct configurations. Below a crossover temperature, the string motion is dominated by simple changes in length and shape. In this low-temperature regime, the system is energetically stable because of its inability to explore all possible topological configurations. This kinetic crossover suggests a generalizable conception of topologically broken ergodicity and limited equilibration.

Our understanding of equilibrium thermodynamics relies on simplifying assumptions about kinetics—for example, the ergodic hypothesis, which postulates that a system can explore all energetically equivalent configurations (*1*). When kinetics are constrained (*2–7*), however, ergodicity can break down on relevant timescales, causing memory effects, glassiness, nonequilibration, or slow equilibration (*8*).

Topological constraints on kinetics are of particular interest in the context of the critical role of topology in much of modern physics and have been examined within the context of various mathematical models (*2*, *4*). The constraints can arise from a partition of the accessible states (or phase space) into topologically distinct subsets, often called topological sectors (*9*, *10*). Kinetics within a sector are topologically trivial; they do not alter the system's topology, contrasting with nontrivial kinetics that allow the system to cross through sectors and change the system's topology. If the latter are constrained, then the system cannot explore all of its configurations and should show deviations from reversible equilibrium thermodynamics. In experimental systems, topologically constrained kinetics were invoked early in the context of soft-matter systems—for example, in macromolecule elasticity, foams, cellular patterns, and the kinetics of continuous networks (*2*)—and this broad topic is closely connected to fundamental questions around equilibration, ergodicity, and memory.

[1]Department of Applied Physics, Yale University, New Haven, CT 06511, USA. [2]Theoretical Division and Center for Nonlinear Studies, MS B258, Los Alamos National Laboratory, Los Alamos, NM 87545, USA. [3]Department of Chemical Engineering and Materials Science, University of Minnesota, Minneapolis, MN 55455, USA. [4]Department of Physics, Yale University, New Haven, CT 06511, USA.
*Corresponding author. Email: peter.schiffer@yale.edu (P.S.); cristiano@lanl.gov (C.N.)
†Present address: Department of Physics, University of Maine, Orono, ME 04469, USA.

Strings in Santa Fe ice

We report the direct visualization of topologically constrained kinetics in a designed nanomagnet array. Such arrays, known broadly as artificial spin ice systems, have displayed a range of exotic collective phenomena and technological potential (*11*, *12*). The particular array geometry that we studied is Santa Fe ice (SFI) (*13*, *14*). The structure of SFI is shown in Fig. 1, A and B, where each element is a single-domain ferromagnetic island with the moment oriented along the long axis as a result of shape anisotropy. The islands are arranged in rectangular plaquettes, with pairs of interior plaquettes (Fig. 1, A, C, and D, light blue shaded areas) surrounded by six peripheral plaquettes. Much of the physics of this system can be understood through the moment configurations at the vertices where islands converge in the lattice (*13*, *14*). The SFI lattice geometry requires that some fraction of the vertices are not in the lowest local energy state, even in the collective ground state. These local excitations have previously been dubbed "unhappy" vertices (*13*, *15*) and are indicated with red dots in Fig. 1, C and D. SFI lends itself to the study of topological kinetics because, as we previously showed (*14*), the lattice geometry forces unhappy vertices to form one-dimensional (1D) strings that can either end within interior plaquettes or form closed loops [(*16*), section S3]. In Fig. 1, C and D, we show these strings as olive lines connecting the unhappy vertices in two realizations of the highly degenerate, disordered ground state of the system (*13*, *14*). Such strings have naturally complex topological properties (*17*), as is readily apparent in a bowl of spaghetti or udon (*18*, *19*).

To probe the physics of SFI, we studied samples composed of stadium-shaped permalloy islands with designed lateral dimensions of 470 by 170 nm, thickness of ~2.5 nm, and lattice spacing of a = 600, 700, and 800 nm (Fig. 1A). The specifics of sample fabrication and characterization are discussed in (*16*), section S1, and have been described previously in (*14*),

in which we also showed that the string [pop]ulation and length distributions are therm[ally] activated at the highest experimentally accessible temperatures. We measured the moment configuration in our samples using x-ray magnetic circular dichroism photoemission electron microscopy (XMCD-PEEM) (*16*), which yielded real-space images of the island magnetic moments (Fig. 1B). When we increased temperature, thermal excitations caused a fraction of the moments to visibly flip in orientation between images, with the rate of flipping increasing with increasing temperature, and we could therefore observe the thermal kinetics of this system. We show results for the a = 600 nm sample, in which the interisland interactions are strongest, in the section on quantifying string motion; the data are consistent for the other lattice spacings (*16*). All data are derived from the same XMCD-PEEM images taken on the same samples that were analyzed in (*14*).

Because the energy cost of a string increases with its length, the disordered ground state corresponds to strings of three unhappy vertices, each on three-island vertices. Therefore, in the ground state, strings are constrained to connecting near-neighbor interior plaquettes (Fig. 1, C and D). In excited states of the system, strings can be longer and can connect interior plaquettes that are not neighboring, or they can form closed loops. In our experimental data, the system approached the disordered ground state at the lowest temperatures, with a residual population of excitations that increased in number for the larger lattice spacings (*14*).

Types of string motion

In considering string kinetics, one must consider the possible motions of the strings within the geometrical constraints imposed by the SFI structure. For any string configuration, the strings can be continuously deformed by bending, elongating, or shrinking them while keeping the endpoints the same. Such deformations do not change the topology of the string configuration and thus keep the system within a single topological sector of available configurations, also known as a homotopy class. In the case of SFI, a homotopy class is defined as the set of all string configurations connecting the same interior plaquettes, in which any member of the set can be transformed to any other member of the set through continuous deformations only. Because the SFI ground state can be realized with many different sets of string connections among the plaquettes, the low-energy configurations of the system can be partitioned into different homotopy classes (Fig. 1, C and D).

By contrast, string configurations that cannot be obtained by continuous bending or deformation of the strings are in different

Fig. 1. The Santa Fe ice (SFI) geometry.
(**A**) Schematic of the lattice, where each element represents a single-domain nanomagnet and the lattice spacing is a. The unit cell (indicated in yellow) has four interior plaquettes (indicated by light blue shading) that are separated by two-island vertices and surrounded by 12 peripheral plaquettes. (**B**) XMCD-PEEM image of SFI, in which all of the islands are either black or white, indicating the magnetic moment direction through its component projected onto the incident x-ray beam direction (red arrow). The lattice is slightly offset from the structure in (A). (**C** and **D**) Illustrations of two SFI disordered ground states, where the excited vertices are indicated by circular red dots. They are in different homotopy classes because the interior plaquettes that are connected by strings are distinct.
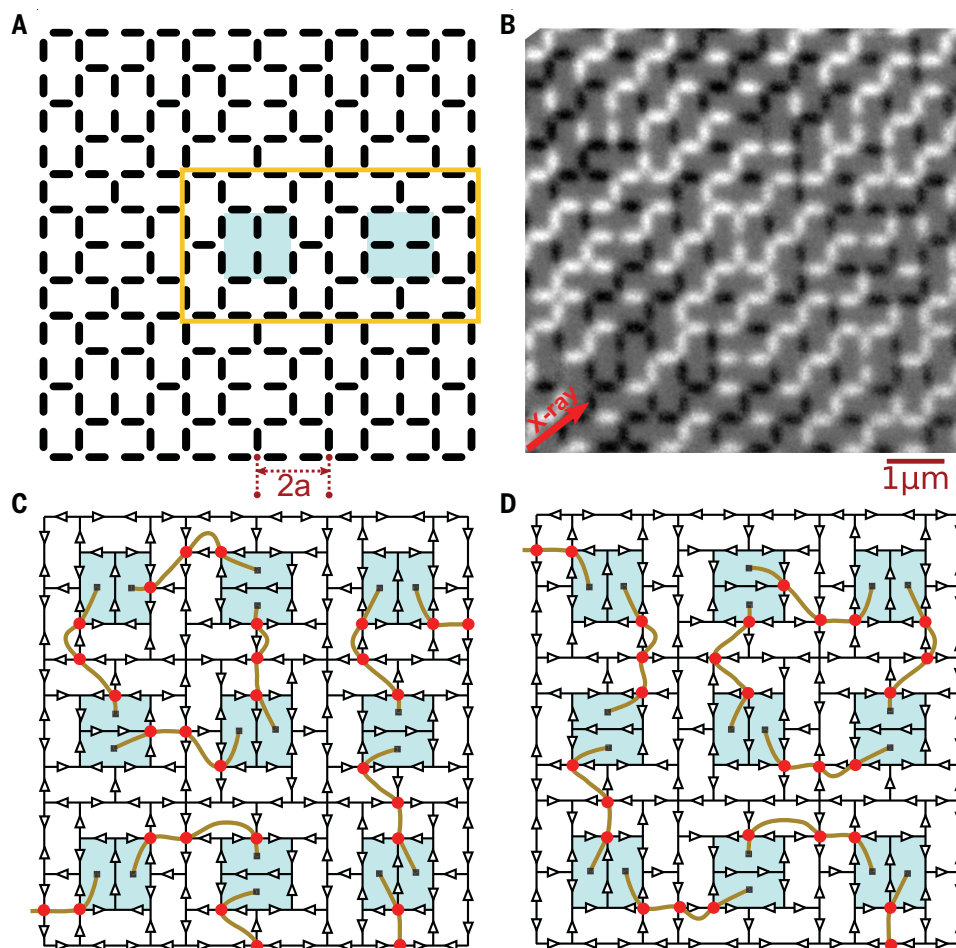
homotopy classes. For example, if two string configurations have different interior plaquettes attached to each other, there is no continuous way to transform the strings from one configuration to another. Strings must be created, eliminated, combined, or cut to transform between such configurations, thus breaking continuity and changing the topology.

In terms of energy, each homotopy class has an energy minimum obtained by continuously deforming and shrinking all the strings in any configuration belonging to the class, so that strings have the minimum number of lowest-energy vertices connecting with the string endpoints. If strings in a homotopy class extend to connect interior plaquettes that are not in close proximity, the energy minimum of that homotopy class is necessarily higher than the global ground state energy. To relax to the ground state, the system requires a topological change in the strings to change the homotopy class. Such a process, in which a string changes in such a way that the system transits from one homotopy class to another, is called "topological surgery" (20, 21). The specific process of topological surgery in SFI occurs when two or

more strings merge and then separate into a new configuration. This concept of topological surgery—the connection and separation of proximate 1D objects—can also be used to describe diverse phenomena such as chromosome meiosis, DNA recombination, magnetic flux reconnection in plasmas, vortex line fusion and reconnection in classical and quantum liquids, and dislocation lines in metallurgy (22–26). SFI provides an unusual opportunity for experimentally tracking this process in real time in a thermal system.

On the basis of the topological character of the strings in SFI, we considered the kinetics of our string configurations. We analyzed these kinetics by comparing sequential XMCD-PEEM images (27, 28) and recording the motions (we use the term "motion" to describe any change to a string, including the creation and annihilation of loops). We classified string motions into two categories: trivial and nontrivial. These two categories correspond to motions that continuously deform a string or to motions that include a change in string topology, respectively. In other words, trivial motions do not change the homotopy class of the string configuration in the

system, whereas nontrivial changes do. The distinction is demonstrated in Fig. 2, where we show simple examples of each, and in Fig. 3, where we give a taxonomy of trivial and nontrivial motions.

The trivial motions of strings correspond to continuous deformations of strings that retain the same interior plaquettes as endpoints. The different variations of trivial motions are shown in the top schematic of Fig. 3 and are labeled "wiggle" [red (T1), dark blue (T2), and purple (T3)]; "grow" and "shrink" [orange (T4)]; "loop": "wiggle" [green (T5)]; "loop": "grow" and "shrink" [light blue (T6)]; and "loop": "creation" and "annihilation" [pink (T7)]. The loop motions are included as trivial because loops are contractible to zero, and thus loop creation and annihilation are topologically trivial.

The nontrivial motions of strings are those changes that represent a change in the homotopy class of the system—that is, a change in how the interior plaquette endpoints are connected by strings. The different variations of nontrivial motions are shown in the bottom schematic of Fig. 3 and are labeled "merge" and "split" [magenta/red (N1/N2) and light

Fig. 2. Trivial and nontrivial string motions. Red dots indicate unhappy vertices. (**A** to **C**) Examples of trivial string motions. Between configurations (A) and (B), there is a "wiggle" motion with no energy change. Between configurations (B) and (C), there is a "grow" motion with energy change because (C) is longer. (**D** to **F**) Examples of nontrivial string motions. Configurations (D) and (F) have pairs of strings that have different pairs of endpoints, and configuration (E) has a merged crossed string with four endpoints. Each of the three configurations represents topologically distinct states, that is, different homotopy classes.
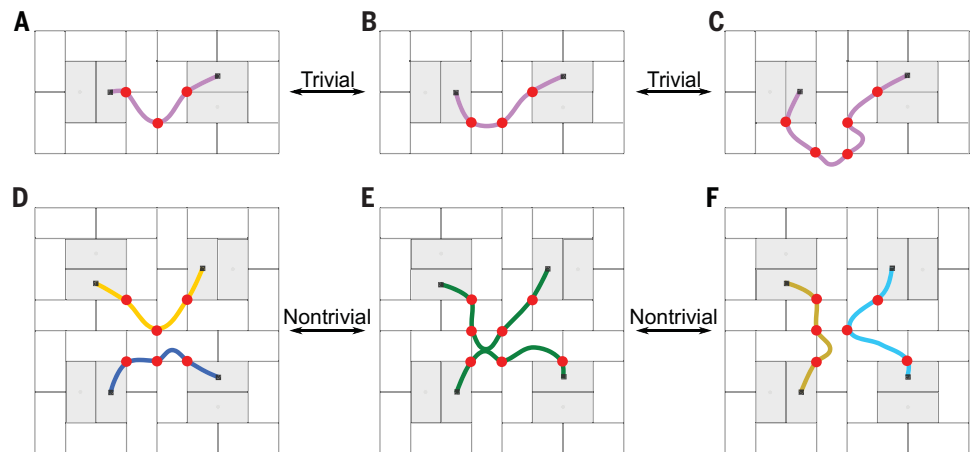
Fig. 3. Illustration and taxonomy of various string motions. Island moments are shown as open arrows, and the flipped island moments (solid arrows) correspond to the strings. (Top) Trivial string motions. (Bottom) Nontrivial string motions. The tables list the motions illustrated in the schematics.

Topologically Trivial String Motions

Topologically trivial motions		
Wiggle	Energy increase (**T1**)	
	Energy decrease (**T1**)	
	No energy change (**T2**,**T3**)	
Grow (**T4**)		
Shrink (**T4**)		
Loop	Wiggle (**T5**)	
	Grow (**T6**)	
	Shrink (**T6**)	
	Creation (**T7**)	
	Annihilation (**T7**)	

Topologically Nontrivial String Motions

Topologically nontrivial motions		
Merge (**N1**,**N2**→**N3**)		
Split (**N3**→**N1**,**N2**)		
Reconnection (**N4**,**N5**↔**N6**,**N7**)		
Adjacent reconnection (**N8**)		
Strings on adjacent interior plaquette	Creation (**N9**)	
	Annihilation (**N9**)	

purple (N3)]; "reconnection" [green/light blue (N4/N5) and olive/dark blue (N6/N7)]; "adjacent reconnection" [purple (N8)]; and "strings on adjacent interior plaquettes": "creation" and "annihilation" [orange (N9)]. Merge and split are necessarily intermediate steps of a reconnection, but because of the limited time resolution, we labeled a full reconnection distinctly, when we could witness a full reconnection between two consecutive frames. Adjacent reconnection and interior creation and annihilation are in a separate category in that they involve only adjacent interior plaquettes with a shared side and the flip of a single moment along that side. We therefore focus on the topologically nontrivial kinetics

associated with strings that traverse the peripheral plaquettes.

In addition to the trivial and nontrivial string motions that we classified, there are strings that naturally do not change between sequential images (that have no motion). There are also complex motions that involve multiple nontrivial changes in moment orientations between two sequential XMCD-PEEM images, as a consequence of the finite time resolution of image acquisition. Furthermore, there are other trivial and nontrivial motions associated with a small number of nanoislands whose magnetizations could not be determined from our XMCD-PEEM images (<0.1%) or that lie on the edges of those images; these motions

resulted in incomplete strings in our image recognition program. These other motions and complex motions are not listed in the Fig. 3 tables.

Quantifying string motion

To quantitatively and unambiguously characterize the string motions from our sequential experimental maps of the moments, we used an analysis program that labels each string with two sets: One set comprises the interior plaquettes at which the string ends, and the other set comprises the unhappy vertices it connects. By comparing the elements in these two sets between sequential images, the algorithm can therefore collect the temperature-

dependent prevalence of each type of string motion (*16*). We quantified the string-motion prevalence as *N*, the average number of string motions between subsequent XMCD-PEEM images per unit cell. *N* effectively gives the rate of string motions because the images are taken at 1-s intervals, and it can be separated by the type of motion involved.

We then turned to the temperature dependence of our data. We first examined the total vertex energy of the system as a function of temperature, for example, the sum of the magnetostatic energy at each vertex, averaged over all images at a given temperature, as determined by micromagnetic calculations (*16, 29*). The energy, quantified as the excess above the ground state, has a clear crossover temperature of around $T_X = 330$ K (Fig. 4A), which is reflected in the kinetics of the strings and is also visible in our previously published data on average string length in the system (*14*).

In Fig. 4, B to D, we show the statistics of motions as a function of temperature, with the temperature regime below T_X indicated by shading. Below T_X, trivial string motions dominate, whereas nontrivial string motions dominate above T_X (the number of trivial motions at higher temperatures is suppressed by a fraction of them being subsumed within the nontrivial motions). The system energy shown in Fig. 4A is nearly flat below T_X; the system does not substantially change its energy as a function of temperature (even though string motions retain considerable temperature dependence).

This temperature independence is consistent with the observed crossover in the predominant types of string motions from nontrivial to trivial when crossing through T_X. Substantial reductions in system energy require topological changes in the strings—that is, nontrivial motions—and therefore the system is unable to relax to a lower-energy overall configuration.

Among the nontrivial motions above T_X, the complex motions are predominant (Fig. 4C). Because these represent multiple updates of the moments among XMCD-PEEM images at higher temperature, they also include most other topologically nontrivial motions. By contrast, local processes among adjacent interior plaquettes dominate below T_X (Fig. 4D). This is consistent with the system's topological constraints because such motions require only a single moment flip and make a minimal change to the system's topology.

We next considered the trivial kinetics. As shown in Fig. 5A, the loop processes (light green curves) and wiggles (red curves) are the highest contributors. The grow (blue) and shrink (violet) curves always follow each other, as expected from detailed balance. The same can be said in general for all reversible inelastic processes, as seen also in wiggles corresponding to energy increase and decrease (Fig. 5B) (the increase in energy being caused by the strings occupying a vertex of coordination 4, whose excitations have slightly higher energy than vertices of coordination 3) and loop creation and annihilation (Fig. 5C). Most of the wig-

gles, however, do not change the total system energy (Fig. 5B), and thus they dominate (Fig. 5A, red curve).

Last, in Fig. 5D we show a log-linear plot of the number of trivial processes, $N_{trivial}$, versus the reciprocal temperature. Within our fairly narrow accessible temperature range below T_X, the data display apparent thermally activated behavior: $N_{trivial}(T) = \frac{1}{\tau_o} e^{-\frac{E_S}{T}}$, where τ_o is the inverse attempt frequency for the thermal processes and E_S is an energetic barrier for changing states. This apparent activated behavior is also observed for the other lattice spacings (*16*). Fits of that form to the data, however, depend very much on our choice of fitting range, with $\tau_o \sim 10^{-5}$ seconds and $E_S \sim 3000$ K for the $a = 600$ nm sample. We can qualitatively understand this behavior in that the motion of strings, even those with no net energy change, requires moments to flip in direction and overcome the energy barrier associated with the island's shape anisotropy. The energy barrier to flipping a moment, as calculated with micromagnetics at zero temperature, is considerably higher than E_S (*16*), but we expect that the energy barrier for flipping the moment in a real system will be affected by the magnetic texture of the island at elevated temperature (*30*). Similarly, the effective attempt frequency, $1/\tau_o$, is small compared with the typical spin wave frequency, which is in the gigahertz regime. Again, this is perhaps not surprising in that the string motions, even almost all of the trivial ones, are associated with changes in multiple islands.

Fig. 4. Temperature-dependent string properties. The shaded regions indicate the low-temperature regime below T_X. (**A**) The excess energy per unit cell versus temperature. (**B**) The temperature dependence of the average number of string motions per XMCD-PEEM image. We also tracked the number of strings that did not change between subsequent images; we plot the total number of these strings as "no motion." (**C**) The temperature dependence of the average number of string motions per XMCD-PEEM image for all types of nontrivial motions. (**D**) An expanded plot of the low-temperature regime from (C). All data are shown per unit cell and are for $a = 600$ nm SFI; error bars are the SEM from all XMCD-PEEM images taken at the given temperature.
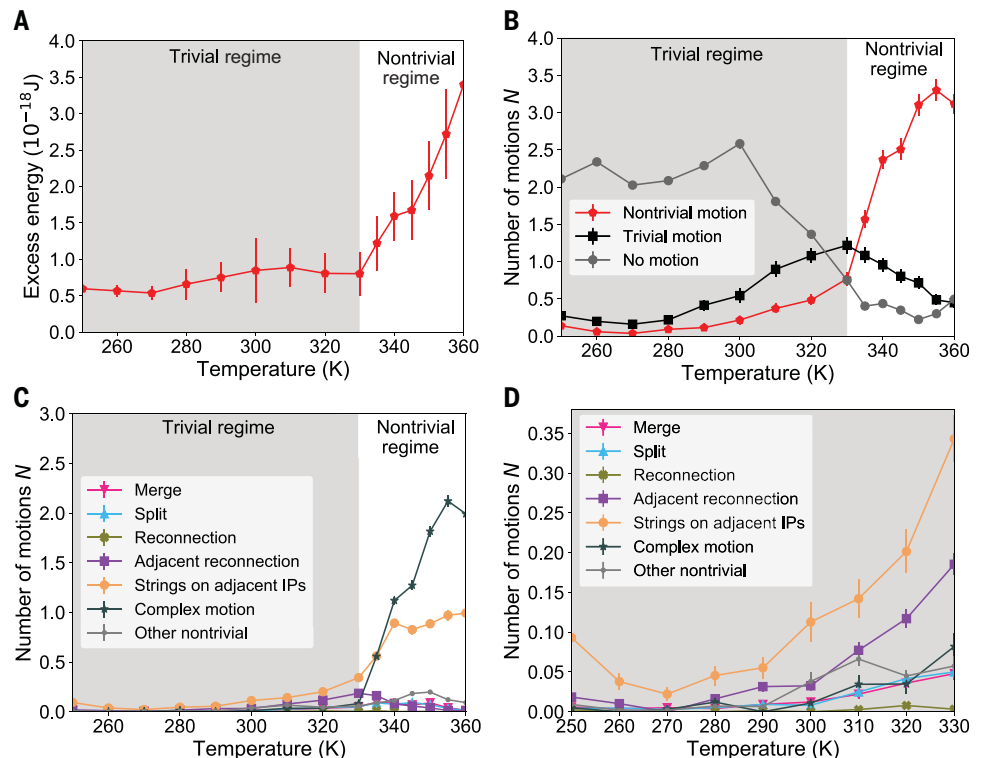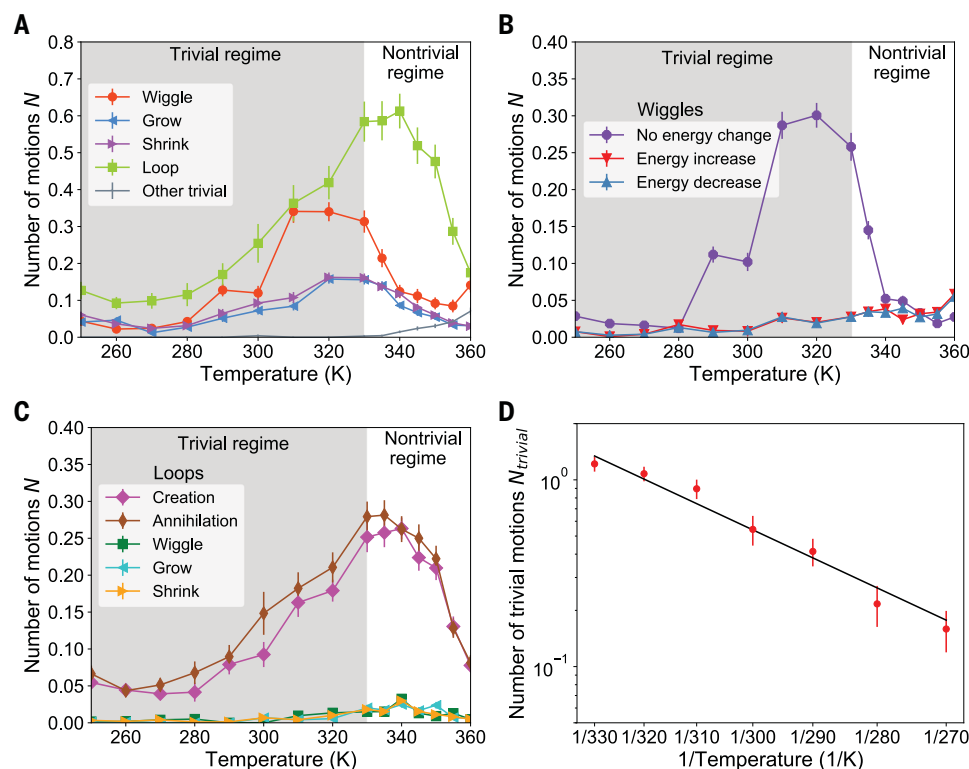
Fig. 5. Temperature dependence of trivial string motions. Shown are the average number of string motions per XMCD-PEEM image for trivial motions. Shading indicates the low-temperature regime in which trivial string motions dominate. (**A**) All types of trivial motions. (**B**) String-wiggle subtypes of trivial motions. (**C**) Loop subtypes of trivial motions. (**D**) The number of total trivial motions as a function of inverse temperature with fit. All data are shown per unit cell and for the a = 600 nm sample. The error bars are the SEM from all XMCD-PEEM images taken at the given temperature.

Discussion and outlook

Our observed crossover leads to a consistent picture of how string kinetics evolve. Below T_X, the system does not change its energy, but it is kinetically active through topologically trivial motions (bending and stretching modes). In this regime, the system has a low likelihood of undergoing topological surgery and changing between homotopy classes. In other words, the system's limited ability to explore homotopy classes likely prevents full ergodicity on experimental timescales at low temperatures, and thus the system is impeded from further reducing its global energy to fully realize the ground state. The trivial kinetic processes are thermally equilibrated below T_X, but within a limited phase space of possible string configurations. This state is evidenced by the close tracking of energy-increasing and -decreasing motions (Fig. 5, A to C), which indicates that detailed balance holds, and by the activated behavior shown in Fig. 5D.

By contrast, at high temperature, above T_X, the topologically nontrivial motions become predominant, and the system appears to be fully ergodic. This allows the total energy of the system to change substantially because the different homotopy classes can have radically different energies; this is the regime in which the activated string length was demonstrated previously (*14*).

The observation of a clear crossover between the two regimes correlates somewhat to glass transitions and other dynamic slowdowns, but here it is driven by topology rather than by a disordered potential landscape. We can broadly understand the crossover in that the homotopy class–changing nontrivial motions require substantially longer strings and thus more moments to reverse directions than do the trivial motions, and therefore are kinetically suppressed with decreasing temperature. Although our present data does not allow us to identify the crossover with a dynamic phase transition and associated nonanalytic behavior, the relative sharpness of the crossover is notable relative to most glass transitions, suggesting future studies with frequency-sensitive techniques (*31–33*).

Our findings should be generalizable in defining and characterizing kinetic crossovers to nonergodicity beyond systems with topological constraints (*34*). Comparing experimental results with existing theoretical methods to ascertain ergodicity could elucidate slow relaxation after quenches and memory effects and aid in exploring the relation with other kinetic crossovers (*8, 34–36*). Such studies could also have relevance for new forms of computing (*37*)

and possibly for quantum tunneling through homotopy classes within qubit realizations (*38*) of SFI or similar structures. Our work might also prove pertinent to systems such as structural glasses, for which dislocation lines ending in vertices proved to be a useful description (*39–42*). The advantage of our physical realization of SFI is that it allows direct experimental measurements of these phenomena, suggesting future examinations of other bespoke topologically interesting structures.

REFERENCES AND NOTES

1. K. Huang, *Statistical Mechanics* (John Wiley and Sons, 2000).
2. D. Weaire, N. Rivier, *Contemp. Phys.* **25**, 59–99 (1984).
3. P. Goldbart, N. Goldenfeld, *Phys. Rev. Lett.* **58**, 2676–2679 (1987).
4. T. Aste, D. Sherrington, *J. Phys. Math. Gen.* **32**, 7049–7056 (1999).
5. F. Ritort, P. Sollich, *Adv. Phys.* **52**, 219–342 (2003).
6. J.-Y. Xiong *et al.*, *J. Phys. Chem. B* **109**, 5638–5643 (2005).
7. P. Oikonomou, P. Cluzel, *Nat. Phys.* **2**, 532–536 (2006).
8. R. G. Palmer, *Adv. Phys.* **31**, 669–735 (1982).
9. C. L. Henley, *J. Phys. Condens. Matter* **23**, 164212 (2011).
10. C. Nisoli, *Europhys. Lett.* **132**, 47005 (2020).
11. S. H. Skjærvø, C. H. Marrows, R. L. Stamps, L. J. Heyderman, *Nat. Rev. Phys.* **2**, 13–28 (2020).
12. P. Schiffer, C. Nisoli, *Appl. Phys. Lett.* **118**, 110501 (2021).
13. M. J. Morrison, T. R. Nelson, C. Nisoli, *New J. Phys.* **15**, 045009 (2013).
14. X. Zhang *et al.*, *Nat. Commun.* **12**, 6514 (2021).
15. R. L. Stamps, *Nat. Phys.* **10**, 623–624 (2014).
16. Materials and methods are available as supplementary materials.

17. M. D. Frank-Kamenetskii, A. V. Lukashin, A. V. Vologodskii, *Nature* **258**, 398–402 (1975).
18. D. Michieletto, M. S. Turner, *Phys. World* **27**, 28–31 (2014).
19. D. Michieletto, M. S. Turner, *Proc. Natl. Acad. Sci. U.S.A.* **113**, 5195–5200 (2016).
20. J. W. Milnor, in *Proceedings of Symposia in Pure Mathematics*, vol. 3, *Differential Geometry*, C. B. Allendorfer, Ed. (American Mathematical Society, 1961), pp. 39–55.
21. S. Antoniou, S. Lambropoulou, *PLOS ONE* **12**, e0183993 (2017).
22. M. A. Berger, G. B. Field, *J. Fluid Mech.* **147**, 133 (1984).
23. J. Koplik, H. Levine, *Phys. Rev. Lett.* **71**, 1375–1378 (1993).
24. S. Kida, M. Takaoka, *Annu. Rev. Fluid Mech.* **26**, 169–177 (1994).
25. U. F. Kocks, H. Mecking, *Prog. Mater. Sci.* **48**, 171–273 (2003).
26. M. Yamada, R. Kulsrud, H. Ji, *Rev. Mod. Phys.* **82**, 603–664 (2010).
27. A. Farhan *et al.*, *Phys. Rev. Lett.* **111**, 057204 (2013).
28. I. Gilbert *et al.*, *Nat. Phys.* **12**, 162–165 (2016).
29. A. Vansteenkiste *et al.*, *AIP Adv.* **4**, 107133 (2014).
30. S. D. Slöetjes, B. Hjörvarsson, V. Kapaklis, *Appl. Phys. Lett.* **118**, 142407 (2021).
31. M. Pohlit *et al.*, *Phys. Rev. B* **101**, 134404 (2020).
32. M. Goryca *et al.*, *Phys. Rev. X* **11**, 011042 (2021).
33. M. Goryca *et al.*, *Phys. Rev. B* **105**, 094406 (2022).
34. G. Miloshevich, T. Dauxois, R. Khomeriki, S. Ruffo, *Europhys. Lett.* **104**, 17011 (2013).
35. F. Borgonovi, G. L. Celardo, M. Maianti, E. Pedersoli, *J. Stat. Phys.* **116**, 1435–1447 (2004).
36. D. Mukamel, S. Ruffo, N. Schreiber, *Phys. Rev. Lett.* **95**, 240604 (2005).
37. A. Lucas, *Front. Phys.* (Lausanne) doi:10.3389/fphy.2014.00005 (2014).
38. A. D. King, C. Nisoli, E. D. Dahl, G. Poulin-Lamarre, A. Lopez-Bezanilla, *Science* **373**, 576–580 (2021).
39. D. R. Nelson, M. Rubinstein, F. Spaepen, *Philos. Mag. A Phys. Condens. Matter Defects Mech. Prop.* **46**, 105–126 (1982).
40. D. R. Nelson, M. Widom, *Nucl. Phys. B* **240**, 113–139 (1984).
41. S. Sachdev, D. R. Nelson, *Phys. Rev. Lett.* **53**, 1947–1950 (1984).
42. D. R. Nelson, in *Applications of Field Theory to Statistical Mechanics*, L. Garrido, Ed. (Springer, 1985), pp. 13–30.
43. X. Zhang *et al.*, Topological kinetic crossover in a nanomagnet array, Dryad (2023); https://doi.org/10.5061/dryad.w0vt4b8w9.
44. X. Zhang *et al.*, Topological kinetic crossover in a nanomagnet array, version 1, Zenodo (2023); https://doi.org/10.5281/zenodo.7641526.

Topological kinetic crossover in a nanomagnet array

Xiaoyu Zhang, Grant Fitez, Shayaan Subzwari, Nicholas S. Bingham, Ioan-Augustin Chioar, Hilal Saglam, Justin Ramberger, Chris Leighton, Cristiano Nisoli, and Peter Schiffer

Editor's summary

Frustrated magnetic systems, such as spin ices, do not have a ground state in which each spin is at an energy minimum. In an artificial spin ice geometry called Santa Fe ice, this frustration can be viewed through the magnetic moment configurations at the vertices of the magnetic array. X. Zhang *et al.* monitored the kinetics of the strings formed by "unhappy" vertices—those not in their lowest energy state. Using x-ray magnetic circular dichroism photoemission electron microscopy, the researchers took images of the system once a second and analyzed the observed changes in string configurations. The system underwent a crossover between a low-temperature regime with limited string motion to a high-temperature one characterized by changes in string topology. —Jelena Stajic

View the article online
https://www.science.org/doi/10.1126/science.add6575
Permissions
https://www.science.org/help/reprints-and-permissions

Use of this article is subject to the Terms of service